2016

Performance Analysis of a Reciprocating Compressor under Typical Transients of Refrigeration Systems

Marco Carrilho Diniz
POLO - UFSC, Brazil, marcodiniz@polo.ufsc.br

Cesar Jose Deschamps
POLO - UFSC, Brazil, deschamps@polo.ufsc.br

Performance Analysis of a Reciprocating Compressor under Typical Transients of Refrigeration Systems

Marco C. DINIZ[1], Cesar J. DESCHAMPS[1]*

[1]POLO Research Laboratories for Emerging Technologies in Cooling and Thermophysics
Federal University of Santa Catarina
Florianopolis, SC, Brazil
deschamps@polo.ufsc.br

* Corresponding Author

ABSTRACT

The performance of reciprocating compressors is usually evaluated under steady-state operating conditions defined in standards. However, the compressor is submitted to quite different conditions in actual refrigeration systems, such as transients associated with the on/off cycling operation. This paper presents a simulation model developed to evaluate the performance of reciprocating compressors during typical transients of refrigeration systems. The model is formed by the coupling of two sub models, one for the compression chamber and the other to calculate the temperatures and mass flow rates in components other than the compression chamber. As the model only simulates the compressor, experimental data was required to provide input from the remaining components of the system. The model was validated by comparing predictions and experimental data of discharged mass flow rate and power consumption of a compressor operating under two transient system conditions. Then, the simulation model was employed to predict the variation of the compressor efficiencies and temperatures during the typical transients analyzed.

1. INTRODUCTION

About 1.4 billion household refrigerators and freezers are in use worldwide (Barther and Götz, 2012) and virtually all of these refrigerators operate based on the vapor compression refrigeration cycle. The performance of these appliances depends on the efficiency of each of its components, but also on the manner they interact with each other.

Despite the advent of variable speed compressors, the vast majority of the compressors employed on refrigerators are still single speed. In this case, the refrigerator operation is characterized by alternate periods at which the compressor is either operating (on) or idle (off). The analysis of the transient operating conditions of refrigerators has been the subject of several researches during the last 30 years. However, most of such studies have focused their attention either on the heat exchangers or on the throttling device.

Regarding the compressor operation during the refrigerator transients, two main aspects must the addressed. First, and most important, is the variation of the pressure ratio to which the compressor is submitted. Unlike the conditions during the refrigerator pulldown, when the compressor is started in a typical cycling condition of the refrigerator, the time to reach a stabilized pressure ratio is usually short. However, this may differ from refrigerator to refrigerator due to aspects such as the volume of the refrigerated compartment, volume of the heat exchangers, compressor displacement volume, throttling device and refrigerant charge. The second aspect is related to the transient behavior of the compressor temperatures during the on/off cycling conditions, which may vary even when the pressure ratio is already stabilized.

Few studies have been developed regarding the compressor performance under transient refrigerator conditions. Some of these studies focused on the crankshaft mechanism and/or bearing system during the first seconds after

startups and shutdowns (Dufour *et al.*, 1995; Link and Deschamps, 2011). In other studies, the objective was to predict mass flow rate and power consumption (Porkhial *et al.*, 2002; Hermes and Melo, 2008; Ndiaye and Bernier, 2010; Negrao *et al.*, 2011) or heat transfer phenomena (Lohn *et al.*, 2015). None of such works has focused on understanding the phenomena that influence the efficiency of the compressor during typical transients of refrigeration systems.

This paper presents a simulation model developed to characterize the performance of reciprocating compressors under transient system conditions. It consists of two sub models: one to predict the compression chamber and the other to calculate the variation of the temperatures and mass flow rates in components other than the compression chamber. Some input data required for the model were obtained from measurements, which were also used to validate the model predictions.

2. EXPERIMENTAL PROCEDURE

The model developed in this work only simulates the compressor. Therefore, the input parameters that would be calculated by models for the other components of the system had to be experimentally obtained. The required parameters are the evaporating and condensing pressures and the gas temperature at the compressor inlet. Additionally, several parameters were also measured in the experiments to validate model predictions, including the mass flow rate, indicated power, electrical power consumption and compressor temperatures.

The tested system was a one door typical frost-free 300-L refrigerator, in which the compressor is on-off controlled by the freezer temperature, while a mechanical damper is responsible to establish the temperature in the fresh food compartment. The original compressor employed in the refrigerator was substituted by an instrumented compressor with 30% less volumetric displacement than the original and the refrigerant charge (R600a) was set to 27g. The tests were performed with the refrigerator in a controlled environment with temperature of 25ºC and 50% of relative humidity. The refrigerator temperature setting was set to its medium value, at which the freezer temperature reached -16ºC by the time the compressor was switched off.

Two different "on" periods were analyzed in this study. The first was typical of the periodic cyclic operation of the refrigerator. In this case, the equalizing pressure was around 0.8 bar and the "on" cycle had a duration of around 15 minutes. The second period, usually termed recovery on period, takes place immediately after refrigerator defrost. In this case, the equalizing pressure before the compressor is switched on was around 2.6 bar and the "on" period presented a duration of approximately 60 minutes. The transient pressures and suction line temperature that were used as input for the simulation model will be presented and discussed further.

3. MATHEMATICAL MODEL

The model consists of two sub models: one to simulate the compression chamber and the other to calculate the variation of compressor temperatures and mass flow rates. The time scale of the compression cycle (milliseconds) is considerably smaller than that of the compressor thermal transients (minutes), allowing the compression chamber to be simulated using a quasi-steady state approach. The coupled solution procedure will be detailed in section 3.3.

3.1 Compression chamber

The model for the compression chamber follows a transient lumped formulation based on four groups of equations (Todescat *et al.*, 1992). The first group allows the calculation of the instantaneous volume occupied by the gas inside the compression chamber. The second group is the conservation equations applied to the compression chamber. The mass conservation equation is given by:

$$\frac{dm_g}{dt} = \dot{m}_{sv} - \dot{m}_{sv,b} - \dot{m}_{dv} + \dot{m}_{dv,b} - \dot{m}_{pc} \tag{1}$$

In Equation (1), $\dot{m}_{sv}$ and $\dot{m}_{dv}$ are the instantaneous mass flow rates through the suction and discharge valves, while $\dot{m}_{pc}$ represents the instantaneous leakage through the piston cylinder gap and the subscript b indicates backflow in

both valves. With the instantaneous mass and volume of refrigerant inside the compression chamber it is possible to calculate its density.

The instantaneous temperature of the refrigerant inside the compression chamber is obtained by applying the energy conservation equation, given by:

$$\frac{dT_g}{dt} = A - BT_g \tag{2}$$

where

$$A = \frac{1}{m_g c_v}\left[H_g A_w T_w - h_g \frac{dm_g}{dt} + (\dot{m}_{sv} h_{sc}) - (\dot{m}_{sv,b} h_g) - (\dot{m}_{dv} h_g) + (\dot{m}_{dv,b} h_{dc}) - (\dot{m}_{pc} h_g)\right] \tag{3}$$

$$B = \frac{1}{m_g c_v}\left[H_g A_w + \left.\frac{\partial p_g}{\partial T_g}\right|_v \frac{d\forall_{cc}}{dt} - \left.\frac{\partial p_g}{\partial T_g}\right|_v v_g \frac{dm_g}{dt}\right] \tag{4}$$

In the above equations H_g is a convective heat transfer coefficient calculated using the correlation proposed by Annand (1963). The method to estimate the mass flow rates in the above equations will be explained shortly. The temperatures of the suction chamber (T_{sc}), discharge chamber (T_{dc}) and cylinder wall (T_w) are calculated by the model that will be described in section 3.2. With the temperature calculated using Equation (2) and the density of the refrigerant it is possible to estimate the pressure inside the compression chamber by means of a state equation.

The third group of equations is used to estimate the dynamics of the suction and discharge valves. A single degree-of-freedom mass-spring model is employed, with effective force areas being used to characterize the force acting on the valve. Finally, the fourth group of equations predicts the mass flow rates that cross the control volume surface. Mass flow rate through the valves is estimated using the concept of effective flow area to correct the theoretical model for the isentropic flow through a convergent nozzle. Leakage through the piston cylinder gap is estimated by considering a fully developed laminar Couette-Poiseuille flow (Ferreira and Lilie, 1984).

The parameters associated with the compression chamber that are used as input in the other sub model are calculated as shown in Table 1. The mechanical losses $\dot{Q}_b$ and the electrical efficiency η_{ele} were specified based on experimental data previously obtained for the compressor under analysis.

Table 1 Output from the compression chamber model.

Parameter	Calculation
$\dot{W}_{ind}$	$f\oint p_g d\forall_{cc}$
$\dot{m}_s$, $\dot{m}_d$, $\dot{m}_l$, $\dot{m}_{s,b}$ and $\dot{m}_{d,b}$	$f\oint \dot{m}_i dt$, where $i = sv$, $i = dv$, $i = pc$, $i = sv, b$ or $i = dv, b$
T_d	$\frac{1}{\dot{m}_d}\oint \dot{m}_{dv} T_g dt$
T_l	$\frac{1}{\dot{m}_l}\oint \dot{m}_{pc} T_g dt$
$T_{s,b}$	$\frac{1}{\dot{m}_{s,b}}\oint \dot{m}_{sv,b} T_g dt$
$\dot{Q}_{mot}$	$(\dot{W}_{ind} + \dot{Q}_b)/\eta_{ele} - (\dot{W}_{ind} + \dot{Q}_b)$

3.2 Temperatures and mass flow rates through control volumes

To calculate the temperature and mass flow rates inside components other than the compression chamber, transient energy and mass balances were applied to the control volumes presented in Figure 1. The energy balances applied to each control volume are presented in Table 2 in the Appendix. The mass balances can also be deduced through the equations presented in Table 2.

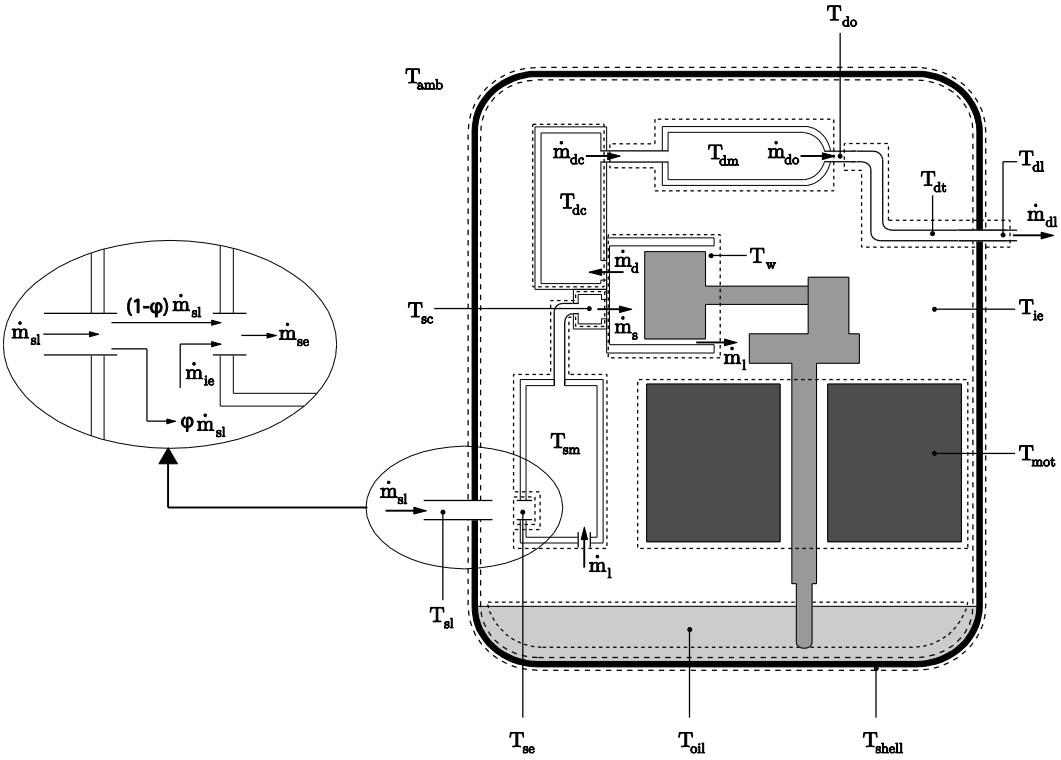

Figure 1: Control volumes for the thermal analysis.

In the compressor employed in this work, part of the gas in the suction line flows directly to the suction muffler, while the other share fills the internal environment (Figure 1). In the model, this flow bifurcation is represented by a factor φ. The φ factor and the heat conductances between the components were obtained by adjusting the model to a measured steady state temperature distribution in a calorimeter, a procedure that has been previously adopted by several other authors, such as Todescat *et al.* (1992). Naturally, the transient terms in the system of equations were not taken into account in this adjustment procedure. The condition chosen for the adjustment consisted on an evaporating temperature $T_e = -28\,°C$ and a condensing temperature $T_c = 40\,°C$ with ambient temperature $T_{amb} = 25$ °C. The adjusted heat conductances and the φ factor were maintained constant throughout the simulation of the compressor under transient conditions.

The nonlinear system of equations represented in Table 2 is solved by means of a Newton-Raphson method. Of especial interest are the suction chamber, cylinder and discharge chamber temperatures, which are used as input data in the compression chamber model.

3.3 Solution procedure

The solution procedure is based on exchange of information between the two previously discussed models. Figure 2 presents the flowchart that characterizes the coupled solution for the overall model. The instantaneous operating conditions are given by the system condensing and evaporating pressures and compressor inlet temperature, obtained from the experimental tests of the refrigerator.

Since the compression chamber and the thermal model require input data from each other, inside each time step an iterative procedure is necessary to verify convergence, which is considered to be reached when the suction chamber temperature and the inlet mass flow rate present a variation between successive iterations of less than 0.1%.

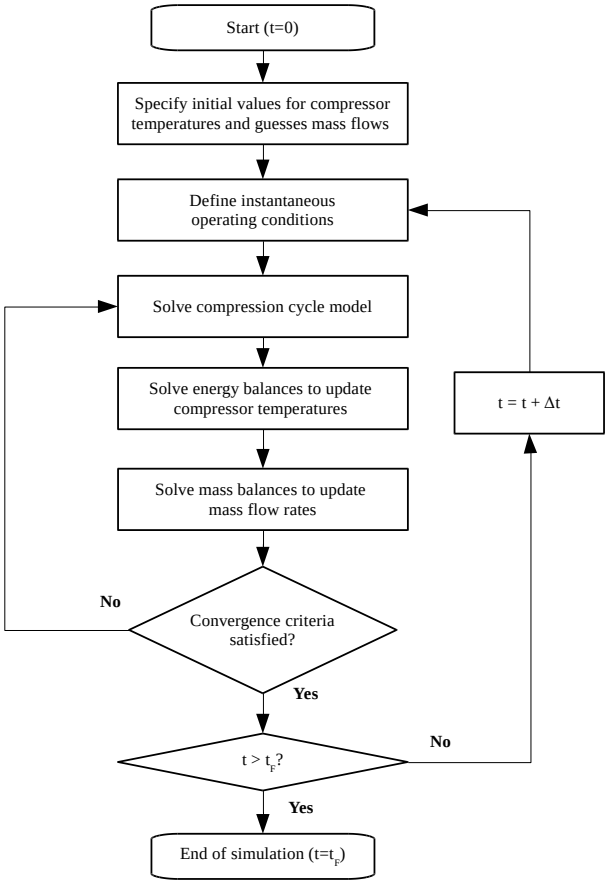

Figure 2: Flowchart of the solution procedure.

4. RESULTS

Figures 3 and 4 present the measured suction and discharge pressures during the two "on" periods considered in this study. The data is normalized by the total time of each period (15 min. and 60 min.). It can be observed that for the typical cycling condition the suction pressure rapidly approaches its stabilized value. On the other hand, the transient associated with the defrost recovery is quite different, and resembles more a refrigerator pulldown.

The transient evaporating and condensing pressures shown in Figures 3 and 4 and the compressor inlet temperature were used as input data for the compressor model. Figures 5 and 6 show the comparison between experimental and numerical results of mass flow rate in the two transients (cycling and defrost recovery), with good agreement being observed for both cases. The discrepancy observed during the first 20 to 30 seconds, only visible in Figure 5, cannot be fully explained at this stage of our study but is more likely to be a result of measurement errors due to the presence of some liquid droplets inside the measurement section of the flow meter. Considering the cycling condition, the results show that the variation of mass flow rate is not significant after a normalized time around 0.2. On the other hand, this variation of mass flow rate is slightly more intense for the defrost recovery condition due to the variation of the suction pressure, as shown in Figure 4.

Figures 7 and 8 present the evolution of electrical power consumption and indicated power during the typical cycling and defrost recovery conditions. As observed for the mass flow rate, the trends of variation are different, with the defrost recovery showing a considerable variation during the whole period. Some discrepancies between

predictions and measurements can be observed for the indicated power, which can partially be attributed to absence of models to predict the pressure pulsations in the suction and discharge systems, as well as to errors in the leakage and heat transfer models. Furthermore, the more significant discrepancies observed for the electrical power consumption can be attributed to lack of appropriate models for the mechanical losses and electrical motor efficiency, but also to the aforementioned discrepancies regarding the indicated power.

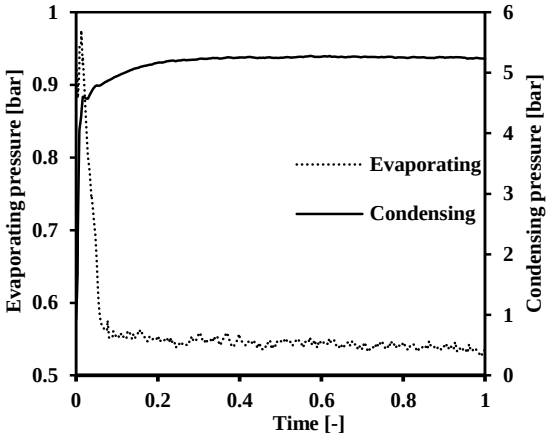

Figure 3: Transient variation of evaporating and condensing pressures for the typical cycling

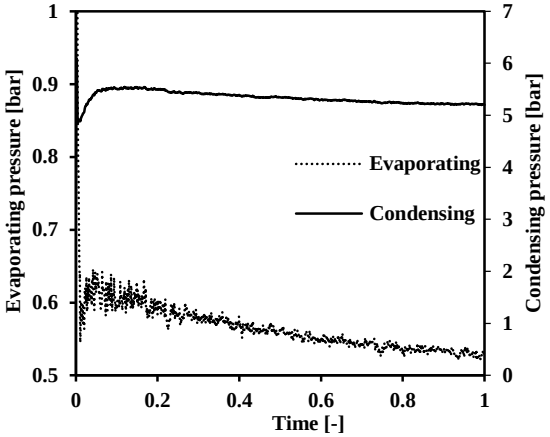

Figure 4: Transient variation of evaporating and condensing pressures for the defrost recovery

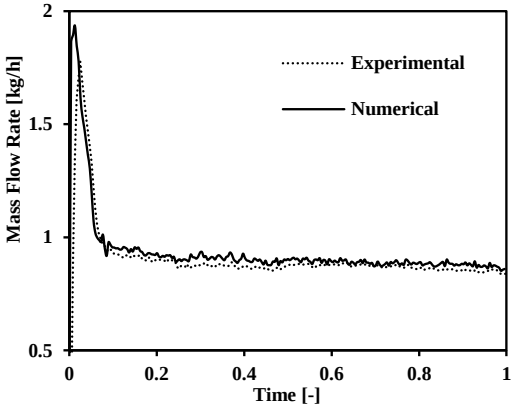

Figure 5: Numerical and experimental results of mass flow rate for the typical cycling

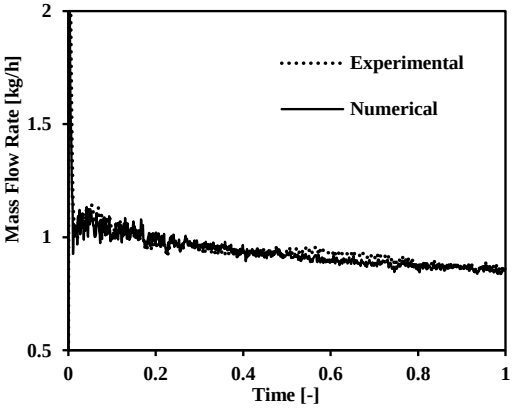

Figure 6: Numerical and experimental results of mass flow rate for the defrost recovery

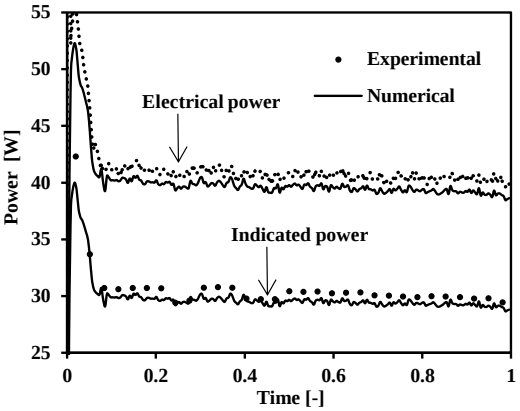

Figure 7: Numerical and experimental results of electrical and indicated power for the typical cycling

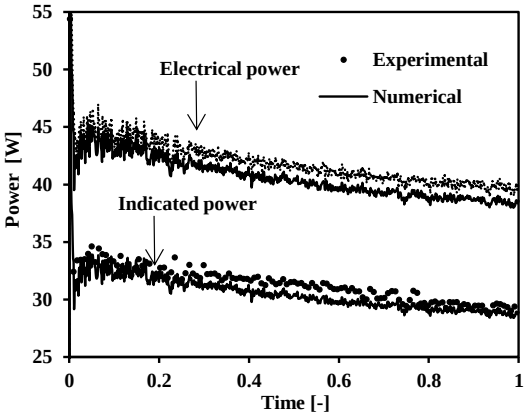

Figure 8: Numerical and experimental results of electrical and indicated power for the defrost recovery

Figure 9 and 10 show the transient variation of the temperatures in suction chamber and at the cylinder wall. Despite the deviations, the trends are well captured by the simulation model, which predicts the temperatures in both conditions with an average error of around 2ºC. In part, the deviations can be attributed to the fact that the heat conductances and the φ factor were maintained constant throughout the transient simulation. These coefficients are expected to vary, especially during the first minutes of compressor operation, due to the considerable variation in the mass flow rate. Therefore, improvements in this methodology will be incorporated in future work.

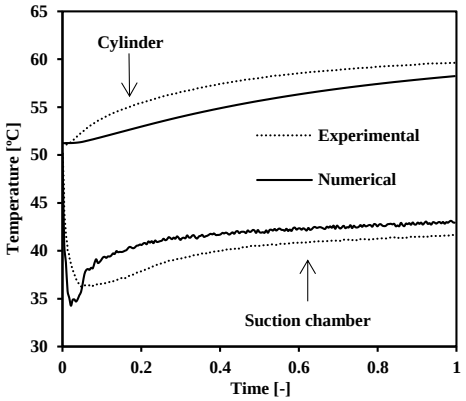

Figure 9: Numerical and experimental results of temperatures in the suction chamber and at the cylinder wall for the typical cycling

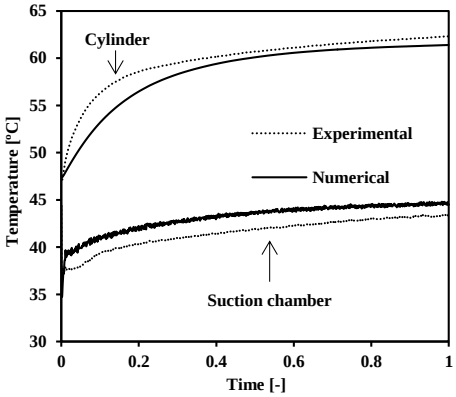

Figure 10: Numerical and experimental results of temperatures in the suction chamber and at the cylinder wall for the defrost recovery

Figures 11 and 12 presents the pressure ratio to which the compressor is submitted and the numerical results of thermodynamic, volumetric and global the efficiencies for the two conditions analyzed. For the cycling condition (Figure 11), the thermodynamic and global efficiencies approach a minimum value in the beginning of the period due to aspects such as suction superheating and losses in the suction and discharge processes. A local minima for these efficiencies is also observed in the defrost recovery moments after the compressor is turned on. However, the global minima for this condition are observed immediately before compressor shut down, mainly as a result of the increase in compressor temperatures. On the other hand, for both conditions, the volumetric efficiency presents a monotonic behavior that is mainly governed by the pressure ratio.

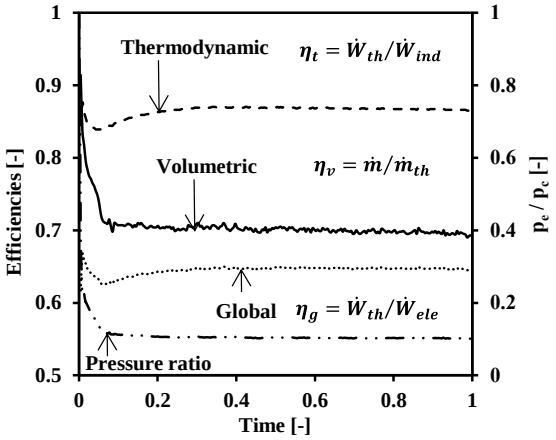

Figure 11: Numerical results of efficiencies for the typical cycling

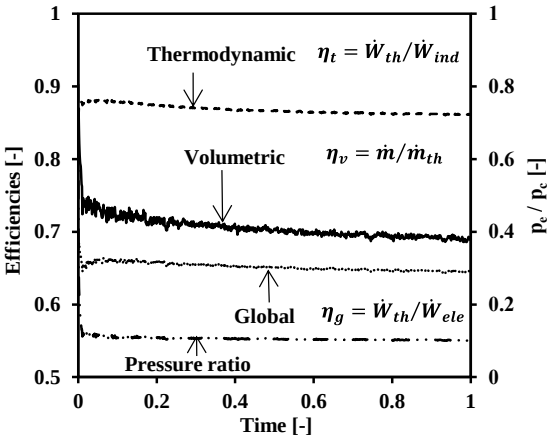

Figure 12: Numerical results of efficiencies for the defrost recovery

Figures 13 and 14 present the effect of suction superheating (ΔT_{sup}) on the thermodynamic power (ϕ) and mass flow rates (ψ) during both transients. The peak of suction superheating reached soon after the compressor is switched on is more intense for the cycling condition. This increases the power necessary the compress the gas by almost 10%, which explains in part the minimum value for the thermodynamic efficiency (Figure 11). The mass

flow rate is also reduced from its theoretical value, but this impact is smaller than that due to the pressure ratio. The results for defrost recovery condition show that the negative effect of the suction superheating increases with time.

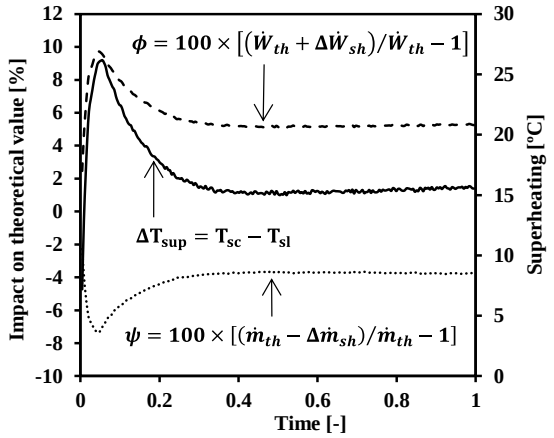

Figure 13: Impact of suction superheating during the cycling on

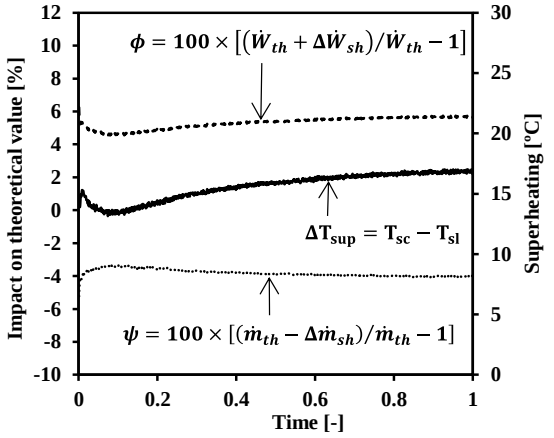

Figure 14: Impact of suction superheating during the recovery on

6. CONCLUSIONS

This paper presented a simulation model to calculate the performance of reciprocating compressors under two transient conditions found in refrigerators, represented by standard cycling and defrost recovery conditions. The model consists of two sub models, one for the compression chamber and the other to predict the compressor temperature distribution and mass flow rates through components other than the compression chamber. A compressor was tested in a refrigerator and several parameters were measured (mass flow rate, indicated power, electrical energy consumption, temperatures). Some of these measurements were used as input data and others to validate the simulation model. Overall, the model was shown to be capable of predicting the transient performance of a compressor in a refrigerator. The results showed that the volumetric efficiency, which is closely related to the pressure ratio, presents a monotonic variation during both transient transients. The thermodynamic and global efficiencies presented a minimum value in the typical cycling condition immediately after the compressor start up. This minimum value was shown to be strongly related to the suction gas superheating. For the recovery on the minimum value of thermodynamic and global efficiencies were found to occur immediately before compressor shutdown.

NOMENCLATURE

General symbols

A	Area	[m^2]	$\dot{Q}_{mot}$	Motor losses	[W]
f	Compressor speed	[Hz]	T	Temperature	[ºC]
H	Heat transfer coefficient	[W/m^{2}K]	T_d	Average discharge temperature	[ºC]
h	Enthalpy	[J/kgK]	UA	Heat conductance	[W/K]
$\dot{m}$	Mass	[kg]	$\forall$	Volume	[m^3]
$\dot{m}$	Mass flow rate	[kg/s]	$\dot{W}_{ind}$	Indicated power	[W]
$\dot{m}_d$	Mass flow rate at discharge orifice	[kg/s]	η_g	Global efficiency	[-]
$\dot{m}_s$	Mass flow rate at suction orifice	[kg/s]	η_t	Thermodynamic efficiency	[-]
p	Pressure	[Pa]	η_v	Volumetric efficiency	[-]
$\dot{Q}$	Heat transfer rate	[W]	φ	Semi-direct suction factor	[-]
$\dot{Q}_b$	Mechanical losses	[W]			

Subscripts

amb	External environment	l	Leakage
b	Related to backflow	mot	Electrical motor
c	Condensing	oil	Lubricant oil

cc	Compression chamber	pc	Piston cylinder gap
d	Averaged value at discharge orifice	s	Averaged value at suction orifice
dc	Discharge chamber	sc	Suction chamber
dl	Discharge line	se	Suction muffler inlet
dm	Discharge muffler	$shell$	Compressor shell
do	Discharge muffler outlet	sl	Suction line
dt	Discharge tube	sm	Suction muffler
dv	Discharge valve	sv	Suction valve
e	Evaporating	th	Theoretical value
ie	Compressor internal environment	w	Compression chamber wall
g	Gas inside compression chamber		

REFERENCES

Annand, W. J. D. (1963). Heat transfer in the cylinders of reciprocating internal combustion engines. *Proc. I. Mech. Eng.* ***117*** *973-96.*

Barther, C. and Götz, T. (2012). *The overall worldwide saving potential from domestic refrigerators and freezers*. Wuppertal, Germany. Wuppertal Institute for Climate, Environment and Energy.

Dufour, R., Hagopian, J. D., & Lalanne, M. (1995). Transient and steady state dynamic behavior of single cylinder compressors: prediction and experiments. *J. Sound Vib.*, 181(1), 23-41.

Hermes, C. J. L. & Melo, C. (2008). A first-principles simulation model for the start-up and cycling transients of household refrigerators. *Int. J. Refrig.*, 31, 1341-1357.

Ferreira, R. T. S. & Lilie, D. E. B. (1984). Evaluation of the leakage through the clearance between piston and cylinder in hermetic compressor. *In: Proc. Int. Compressor Engineering Conference at Purdue University*, (paper 424). West Lafayette, USA.

Lohn, S. K., Diniz, M. C. & Deschamps, C. J. (2015). A thermal model for analysis of hermetic reciprocating compressors under the on-off cycling operating condition. *IOP. Conf. Ser.: Mater. Sci. Eng.*, 90, 012068.

Link, R., & Deschamps, C. J. (2011). Numerical modeling of startup and shutdown transients in reciprocating compressors. *Int. J. Refrig.*, 34, 1398-1414.

Ndiaye, D. & Bernier, M. (2010). Dynamic model of a hermetic reciprocating compressor in on–off cycling operation (Abbreviation: Compressor dynamic model). *Appl. Therm. Eng.*, 30, 792-799.

Negrão, C. O. R., Erthal, R. H., Andrade, D. E. V. & Silva, L. W. (2011). A semi-empirical model for the unsteady-state simulation of reciprocating compressors for household refrigeration applications. *Appl. Therm. Eng.*, 31, 1114-1124.

Phorkial, S., Khastoo & Razavi, M. R. M. (2002). Transient characteristic of reciprocating compressors in household refrigerators. *Appl. Therm. Eng.*, 22, 1391-1402.

Todescat, M. L., Fagotti, F., Prata, A. T. & Ferreira, R. T. S. (1992). Thermal energy analysis in reciprocating hermetic compressors. *In: Proc. Int. Compressor Engineering Conference at Purdue University*, (paper 936). West Lafayette, USA.

ACKNOWLEDGEMENT

The present study was developed as part of a technical-scientific cooperation program between the Federal University of Santa Catarina and EMBRACO. The authors also acknowledge the support of EMBRAPII Unit POLO/UFSC and CAPES (Coordination for the Improvement of High Level Personnel).

APPENDIX

Table 2 Energy balances of thermal hydraulic sub model

CV	$\frac{d}{dt}(mu)$	$\sum \dot{m}h\|_{in}$	$\sum \dot{m}h\|_{out}$	$\sum \dot{Q}$	$\sum \dot{W}$
1	–	$\dot{m}_{ie}h_{ie} + (1-\varphi)\dot{m}_{sl}h_{sl}$	$\dot{m}_{se}h_{se}$	–	–
2	$m_{sm}\frac{u_{sm}^{t+\Delta t}-u_{sm}^{t}}{\Delta t} + u_{sm}\frac{m_{sm}^{t+\Delta t}-m_{sm}^{t}}{\Delta t}$	$\dot{m}_{se}h_{se} + \dot{m}_{s,b}h_{s,b} + \dot{m}_{l}h_{ie}$	$\dot{m}_{s}h_{sc}$	$-UA_{ie-sm}(T_{ie}-T_{sm})$	–
3	$m_w cp_w \frac{T_w^{t+\Delta t}-T_w^{t}}{\Delta t}$	$\dot{m}_{s}h_{sc} + \dot{m}_{d,b}h_{dc}$	$\dot{m}_{s,b}h_{s,b} + \dot{m}_{d}h_{d} + \dot{m}_{l}h_{l}$	$UA_{w-oil}(T_w - T_{oil})$	$\dot{W}_{ind} + \dot{Q}_b$
4	$m_{dc}\frac{u_{dc}^{t+\Delta t}-u_{dc}^{t}}{\Delta t} + u_{dc}\frac{m_{dc}^{t+\Delta t}-m_{dc}^{t}}{\Delta t}$	$\dot{m}_{d}\bar{h}_{d}$	$\dot{m}_{dc}h_{dc} + \dot{m}_{d,b}h_{dc}$	$UA_{dc-ie}(T_{dc}-T_{ie})$	–
5	$m_{dm}\frac{u_{dm}^{t+\Delta t}-u_{dm}^{t}}{\Delta t} + u_{dm}\frac{m_{dm}^{t+\Delta t}-m_{dm}^{t}}{\Delta t}$	$\dot{m}_{dc}h_{dc}$	$\dot{m}_{dm}h_{do}$	$UA_{dm-ie}(T_{dm}-T_{ie})$	–
6	$m_{dt}\frac{u_{dt}^{t+\Delta t}-u_{dm}^{t}}{\Delta t} + u_{dt}\frac{m_{dt}^{t+\Delta t}-m_{dt}^{t}}{\Delta t}$	$\dot{m}_{dm}h_{do}$	$\dot{m}_{dl}h_{dl}$	$UA_{dt-ie}(T_{dt}-T_{ie})$	–
7	$m_{mot}cp_{mot}\frac{T_{mot}^{t+\Delta t}-T_{mot}^{t}}{\Delta t}$	–	–	$UA_{mot-ie}(T_{mot}-T_{ie})$ $-Q_{mot}$	–
8	$m_{oil}cp_{oil}\frac{T_{oil}^{t+\Delta t}-T_{oil}^{t}}{\Delta t}$	–	–	$UA_{oil-shell}(T_{oil}-T_{shell})$ $-UA_{w-oil}(T_w-T_{oil})$	–
9	$m_{shell}cp_{shell}\frac{T_{shell}^{t+\Delta t}-T_{shell}^{t}}{\Delta t}$	–	–	$UA_{shell-amb}(T_{shell}-T_{amb})$ $-UA_{oil-shell}(T_{oil}-T_{shell})$ $-UA_{ie-shell}(T_{ie}-T_{shell})$	–
10	$m_{ie}\frac{u_{ie}^{t+\Delta t}-u_{ie}^{t}}{\Delta t} + u_{ie}\frac{m_{ie}^{t+\Delta t}-m_{ie}^{t}}{\Delta t}$	$\varphi\dot{m}_{sl}h_{sl} + \dot{m}_{l}h_{l}$	$\dot{m}_{l}h_{l} + \dot{m}_{ie}h_{ie}$	$UA_{ie-shell}(T_{ie}-T_{shell})$ $+UA_{ie-sm}(T_{ie}-T_{sm})$ $-UA_{dc-ie}(T_{dc}-T_{ie})$ $-UA_{dm-ie}(T_{dm}-T_{ie})$ $-UA_{dt-ie}(T_{dt}-T_{ie})$ $-UA_{mot-ie}(T_{mot}-T_{ie})$	–